European Polymer Journal 84 (2016) 188–204

Contents lists available at ScienceDirect

European Polymer Journal

journal homepage: www.elsevier.com/locate/europolj

Macromolecular Nanotechnology

Interfacial behavior of PAMAM-PCL dendrimers and *in situ* spontaneous formation of gold nanoparticles at the toluene-water and air-water interfaces: Experimental and theoretical studies

César Saldías [a,*], Maximiliano Méndez-López [a], Mario Saavedra-Torres [b], Alfredo Pereira [c], Moisés A. Rojas [c], Fabián Avila-Salas [c], Sebastián Bonardd [a], Maximiliano Pino-Orellana [a], Soledad Saldías [a], Caterina Quezada [a], Angel Leiva [a], Deodato Radic [a]

[a] Departamento de Química Física, Facultad de Química, Pontificia Universidad Católica de Chile, Casilla 302, Correo 22, Santiago, Chile
[b] Laboratorio de Química Teórica, Departamento de Ciencias del Ambiente, Facultad de Química y Biología, Universidad de Santiago de Chile (USACH), Casilla 40, Correo 33, Santiago, Chile
[c] Laboratory of Asymmetric Synthesis, Institute of Chemistry and Natural Resources, Universidad de Talca, Av Lircay S/N Talca, Maule, Chile

ARTICLE INFO

Article history:
Received 29 June 2016
Received in revised form 1 September 2016
Accepted 9 September 2016
Available online 14 September 2016

Keywords:
Amphiphilic dendrimers
Interfacial tension
Gold nanoparticles
Gibbs adsorption

ABSTRACT

Using pendant drop and Langmuir techniques, the interfacial behavior of hydroxyl-terminated poly(amido amine) (PAMAM-OH) dendrimers of generation 4, modified with poly(ε-caprolactone) (PAMAM-PCL), were analyzed and characterized. The study was performed at the toluene-water and air-water interfaces using two different molecular weights of PAMAM-PCL. Using this method, the interfacial activity of the dendrimers is shown to depend on the chain length of the PCL blocks. Using the Gibbs equation, the driving force for the adsorption process at the toluene-water interface was found to be of an enthalpic nature. In addition, stable monolayers of PAMAM-PCL at the air-water interface were obtained. For this analysis, the elasticity and critical exponent of the excluded volume, ν, for the PAMAM-PCL spread monolayers were determined. Alternatively, when the pure water phase was changed to an $AuCl_4^-$ aqueous solution for both interfaces, different behavior in the interfacial activity of PAMAM-PCL was detected. Moreover, the spontaneous formation of gold nanoparticles at room temperature, at both interfaces, was observed. This was confirmed by UV–vis spectra and atomic force microscopy (AFM) images. Finally, molecular simulations and electronic structure calculations helped us to gain insights on the behavior of the dendrimers at the toluene-water interface and the PAMAM-PCL-gold nanoparticle interactions, respectively.

1. Introduction

The study of interfacial properties at the liquid/liquid and gas/liquid interfaces of diverse compounds is an interesting research field because it addresses many technological and industrial applications, including pharmaceutical [1] and

* Corresponding author.
E-mail address: casaldia@uc.cl (C. Saldías).

http://dx.doi.org/10.1016/j.eurpolymj.2016.09.017
0014-3057/

emulsion formulations [2], food [3], medicine [4], energy [5], membranes [6] and so on. In this context, the interfacial activity of polymeric materials at different interfaces has attracted considerable scientific interest in recent decades [7–9]. These types of materials constitute a highly promising alternative for the design of innovative devices with interesting interfacial properties that can be potentially be exploited in technological applications. Two very useful experimental methods to assess interfacial activity at the liquid/liquid and gas/liquid interfaces of polymers are the pendant drop and Langmuir techniques, respectively [10–14]. Specifically, the interfacial tension between two immiscible liquids can be calculated from the drop profiles of liquid 1 (L1) immersed in liquid 2 (L2), assuming that the polymer is found to be spread at the L1/L2 interface [15,16]. For the Langmuir experiments, surface pressure variations, as a function of the surface concentration of spread polymer monolayers at the air/water interface, are monitored [17,18]. Due to the importance of these properties in diverse applications, theoretical predictions on the activity of polymers at interfaces, derived from scaling theories and mean field approximations, have been contrasted with experimental techniques, such as neutron reflectivity and ellipsometry [19–22]. Recent studies based on atomistic models have been used to simulate amphiphilic dendrimers at liquid-liquid and liquid-air interfaces [23–25]. Such studies aim to provide suitable explanations, at the atomic or molecular level, for the phenomena experimentally observed. On this basis, the chemical modification of polymers could produce the variation of their affinity for any of the phases that are present, enabling potential control of polymer behavior at interfaces [26–28].

Alternatively, dendrimers are a unique type of polymer with three-dimensional globular shapes due to their highly branched architectures and monodispersity [29,30]. Such tree-like conformations allow the free energy of the dendrimeric structures to be minimized, thereby affecting the macromolecular properties. Considering this, a special interest in studying dendrimeric architectures to gain additional insights into their properties has recently emerged [31,32]. Compact globular shapes and sizes, and significant peripheral functionalities, are ideal features for a wide range of applications at surfaces and interfaces [33,34]. For example, the surface activity of amphiphilic dendrimer monolayers by the Langmuir technique has been studied in order to understand the interfacial and physical properties of dendrimers confined at the air/water interface [35–37]. These studies focus on the development of functional materials, such as multilayer membranes for use in sensor devices [38,39]. Additionally, the numerous peripheral functional groups of the dendrimer would enable chemical modification or incorporation of small ligands, drugs, ionic species or additional functionalization [40–43]. Moreover, dendrimers with amphiphilic behavior could be obtained by polymerization onto peripheral functional groups [44,45]. In this context, PAMAM-OH dendrimer could act as macroinitiators for the ring-opening polymerization of biodegradable polyethers and polyesters (e.g. poly (ethylene glycol) (PEG) and poly (ε-caprolactone) (PCL)) to form highly branched non-linear architectures [46,47].

Based on current knowledge, the design of synthetic methods directed towards metal nanoparticles with specific characteristics has attracted significant attention in recent years [48–51]. These methods include several special conditions for the synthesis of metal nanoparticles, such as oil microemulsions in water, micelles as nanotemplates, porous membranes and Langmuir–Blodgett films [52–55]. The spreading of different materials at interfaces has also been used for the synthesis of metal nanoparticles. For example, monolayers of diverse surfactants have been used in the reduction of aqueous silver nitrate solutions to obtain films containing silver nanoparticles [56]. The formation of gold nanostructures embedded into amphiphilic vitamin C has also been reported [57]. This indicates that amphiphilic compounds are ideal for synthesis processes that are kinetically controlled. To the best of our knowledge, comparative studies on the spontaneous reduction of $AuCl_4^-$ ions to produce gold nanoparticles at different interfaces have not yet been completed. Moreover, the use and characterization of hydrophobically modified dendrimers under such experimental conditions is also a topic that has been scarcely explored. In this work, we have focused our attention on the interfacial behavior of PAMAM-PCL dendrimers, in order to achieve a better understanding of their role in the spatially confined synthesis of gold nanoparticles. In addition, molecular dynamics simulations and electronic structure calculations were carried out to provide deeper insights into the behavior of the dendrimers at interfaces and the interactions of dendrimers-gold nanoparticles, respectively. Thus, we expect to contribute in the rational design of dendrimers having amphiphilic tailored properties, in order to achieve an adequate activity and stability at different interfaces [36,58].

2. Experimental

2.1. Materials

ε-caprolactone, hydroxyl-terminated poly (amido amine) generation 4 (PAMAM-OH G4 14,200 g/mol), poly (ε-caprolactone) (PCL 2000 g/mol), tin(II) 2-ethylhexanoate and potassium tetrachloroaurate ($KAuCl_4$) were purchased from Sigma-Aldrich. $CHCl_3$, $CDCl_3$ and toluene solvents were purchased from Merck.

ε-caprolactone was distilled under reduced pressure prior to use. PAMAM-OH G4 was dried by removing the solvent under vacuum for 48 h. The water used in all experiments was purified by a Millipore Milli-Q system (resistivity higher than 18.2 MΩ cm). All other chemicals were used without prior treatment.

2.2. Synthesis and characterization of PAMAM-PCL

The synthesis of PAMAM-PCL containing a core of PAMAM and PCL chains was performed using a previously reported method [46] with minor modifications in the synthetic route. The monomer of ε-caprolactone was polymerized by

ring-opening onto the PAMAM-OH G4 dendrimer in order to obtain the respective PAMAM-PCL hyperbranched dendrimer. Briefly, PAMAM was placed into a glass flask, carefully dried and purged with nitrogen gas prior to use. Later, the ε-caprolactone monomer and tin (II) 2-ethylhexanoate, as a catalyst, were added. The feed ratios of PAMAM-OH G4, ε-caprolactone and tin (II) 2-ethylhexanoate (PAMAM-OH G4/ε-caprolactone/tin (II) 2-ethylhexanoate) were 1/3/0.05 and 1/7/0.05 (w/w/w). The reaction flask was put in an oil bath and vigorously stirred at 378 K for 48 h under N_2 atmosphere. Then, the obtained solid was dissolved in chloroform and further precipitated using cold methanol. This procedure was repeated three times. The obtained samples were dried under vacuum for 72 h at 35 °C. The samples were labeled as G4LPCL and G4HPCL for the lower and higher dendrimer molecular weights, respectively. The entire synthesis procedure was performed in triplicate to ensure reproducibility.

In order to determine the molecular weight of the PAMAM-PCL dendrimers, a static light scattering (SLS) unit Dawn EOS system with an Optilab DSP interferometric refractometer, both from Wyatt Technology, connected in-line with three size exclusion chromatographic (SEC) columns (absolute method for determining of average molecular weights of polymers) was used. The solvent used as eluent was $CHCl_3$. The *dn*/*dc* values were determined by the interferometric refractometer. The *dn*/*dc* values for G4LPCL and G4HPCL were 0.034 and 0.039 mL/g, respectively. The characterization of the dendrimer samples was performed by a Vector Bruker infrared spectrophotometer (FTIR) using the KBr pellet technique. Additionally, nuclear magnetic resonance (^{1}H NMR) spectrum was recorded in a Bruker ACP-200 system using $CDCl_3$ as the solvent.

2.3. Interfacial tension measurements

The interfacial tension of the PAMAM-PCL dendrimers at the toluene-water interface was measured using the pendant drop method (OCA20, Dataphysics). The measurements of interfacial tension were carried out by the acquisition of processed computational images of the drop profile formed inside of a cuvette, which were then fitted to the Laplace–Young equation [59]. The measurements were performed with a water drop (Milli-Q water) immersed in a toluene solution of the PAMAM-PCL dendrimers. For the experiments with $AuCl_4^-$ ions, a drop of potassium tetrachloroaurate ($KAuCl_4$) 5 μg/mL aqueous solution was also immersed into the toluene solution of dendrimers. In the absence of dendrimers, the toluene-water interfacial tension remained constant at values of 34.8 and 34.1 mN m^{-1} for pure water phase and $KAuCl_4$ aqueous solution phase, respectively. For these experiments, the dendrimer concentrations used were 0.01, 0.07, 0.12, 0.21, 0.32, 0.71 and 1.03 mol $L^{-1} \times 10^3$.

2.4. Surface pressure–area isotherms

In order to obtain the surface pressure–area isotherms (π–A), a computerized Langmuir trough Nima Technology model 611 equipped with a mobile barrier and a pressure surface sensor was used. Monolayers were achieved by spreading 100 μL of 0.5 mg/mL PAMAM-PCL in chloroform on water using a Hamilton Microsyringe. After 20 min of solvent evaporation, the monolayers at the air-water interface were compressed with a rate of 10 cm^2/min. Similarly, dendrimer monolayers of both PAMAM-PCL samples were also spread on aqueous solutions of 5 μg/mL $KAuCl_4$ as the subphase.

2.5. Absorbance measurements

To verify the formation of gold nanoparticles at the interfaces studied, UV–vis spectra were recorded between 400 and 800 nm at 25 °C with a Agilent Cary 60 spectrophotometer. In the case of the toluene-$AuCl_4^-$ aqueous solution interface, the solvents were completely evaporated under vacuum to avoid any possible interference of the mixed solvents in the measurements. Then, the formed gold nanoparticles were resuspended in Milli-Q water to obtain the UV-spectra.

2.6. Atomic force microscopy (AFM)

The AFM images were obtained by an AFM Dimension 3110-Nanoscope using the tapping mode. With a microsyringe, a determined sample volume was directly taken from either a Langmuir trough or cuvette, and then deposited onto a silicon wafer to form films with or without gold nanoparticles. After this, evaporation of the solvent was carried out under vacuum at room temperature for 30 h.

2.7. Theoretical methods

2.7.1. Building of molecular structures

Alternately, each peripheral hydroxyl group of PAMAM-OH was functionalized with three monomeric units of ε-caprolactone (32 monomers in total per dendrimer according to the G4LPCL structure) to build PAMAM-PCL molecules, using the *tleap* module of the AmberTools package [60].

2.7.2. Molecular dynamics simulations

In order to obtain information on the molecular behavior of PAMAM-PCL dendrimers at the toluene-water interface, two all-atom molecular dynamics (MD) simulations were performed.

First of all, a PAMAM-PCL dendrimer was incorporated at the center of a 12.0 × 12.0 × 6.5 nm (the x-, y-, and z-directions, respectively) box, a water sub-box and a 12.0 × 12.0 × 6.5 nm toluene sub-box. Secondly, a PAMAM-OH dendrimer was incorporated at the center of a 9.0 × 9.0 × 5.0 nm box, a water sub-box and a 9.0 × 9.0 × 5.0 nm toluene sub-box. In both cases, the dendrimers were placed in the middle of the interface, so that half of the dendrons were distributed in each solvent. The amounts of water and toluene molecules were obtained on the basis of the corresponding molecular experimental density (1 g/cm^3 for water and 0.867 g/cm^3 for toluene). The systems were built using the molecular packing program PACKMOL [61]. MD simulations were run using the Desmond software (Desmond/Maestro academic version 2015.4) [62] and analyzed using VMD 1.9.2 software [63].

The box type was orthorhombic with a boundary distance of 0.1 nm for the two systems previously solvated (no ionic species were added). The systems were relaxed with the default multistage protocol in Desmond, followed by a series of short NVT (constant number, volume and temperature) and NPT (constant number, pressure and temperature) simulations at T = 10 K with varying constraints on solute and solvent atoms [64].

MD production runs were carried out in the NPT ensemble for 24.0 ns for each dendrimer. The temperature was regulated at 300 K with the Nose–Hoover chain thermostat [65,66] with a relaxation time of 1 ps. Pressure was regulated at 1 bar with the Martyna–Tobias–Kleinbarostat using isotropic coupling and a relaxation time of 2.0 ps [67]. The reference system propagator algorithms (RESPA) integrator [68] was used to integrate equations of motions with a 2.0 fs time step for bonded and short-range interactions and a 6.0 fs time step for long-range interactions. A cut-off of 9.0 Å was applied to non-bonding interactions. The smooth particle mesh Ewald method [69] was used to deal with long-range electrostatic interactions with a tolerance of 10^{-9}. The OPLS force field [70] was applied to the system and the TIP3P water model [71] was used.

2.7.3. Radius of gyration and solvent accessible surface area (SASA)

The unfolding behavior of dendrimer structures in solution was characterized using the radius of gyration [72] and SASA [73] parameters. These parameters assess the compactness of a structure according to the relation of each atom with respect to the center of mass of the molecule and the total structure surface in contact with the solvent, respectively. For both the PAMAM-OH and PAMAM-PCL systems at the toluene-water interface, we obtained a total of 5000 conformations from the MD trajectories. Thus, all respective values from these trajectories were calculated using the VMD software [74] and then plotted using the Gnuplot 4.4 software [75].

2.7.4. Density functional theory (DFT) calculations

For all DFT electronic structure calculations, the Gaussian 09 package [76] was used. The hybrid exchange-correlation functional, B3LYP, level of approximation was combined with the Stuttgart quasi-relativistic effective core potential MWB60 basis set for Au atoms along with def2-SVP for the lighter atoms (O, C and H) of the monomer models [77]. One-, two- and three-dimensional (1D, 2D and 3D) structures, represented by Au_1, Au_9 and Au_{13}, respectively, were designed to perform the calculations. As previously reported in the literature, Au_9 and Au_{13} represent planar and 3D structures, respectively [78–80].

The geometry optimization procedure for the monomer-Au_n complexes was carried out by placing the monomers over multiple adsorption sites, initially at a determined distance from the Au_n structure. The complexes that were energetically most stable were chosen and analyzed. These optimized structures were corroborated by vibrational analysis. In this case, two models of the PCL monomer were considered, one containing an (i) ester group and one with an (ii) carboxylic acid group, which are referred to as PCLe and PCLc, respectively.

The complexation energies of the monomer-Au_n systems were calculated by the following equation:

$$\Delta E_{complexation} = E_{monomer\text{-}Au_n} - [E_{Au_n} + E_{monomer}] \quad (1)$$

n = 1, 9 or 13
monomer = PCLe or PCLc

where $E_{monomer\text{-}Au_n}$, E_{Au_n} and $E_{monomer}$ are the ground state energies of the monomer-Au_n complex, Au_n free cluster and free monomer model, respectively. Additionally, a CM5 charge analysis [81,80] (q) was performed to characterize the possible charge involved in the monomer-Au_n systems. In addition, a PCM solvent implicit model was incorporated to compute complexation energies and charges (referred to as $\Delta E_{complexationSol}$ and q_{Sol}, respectively) by simulating a water environment over vacuum optimized structures.

3. Results and discussion

3.1. Characterization of dendrimers

^{1}H NMR and FTIR spectroscopy were used to characterize the PAMAM-PCL dendrimers. Fig. S1† shows the schematic chemical structure of G4LPCL and its respective ^{1}H NMR spectrum. The spectrum confirms that PCL was polymerized onto the peripheral-OH groups of PAMAM. The main signals observed were the methylene groups from both PAMAM and PCL. The

number-average molecular weights ($\overline{M}_n$) and the respective polydispersity indices for the dendrimer samples were determined by static light scattering (SLS) using $CHCl_3$ as the eluent. As ε-caprolactone monomers were polymerized onto the PAMAM-OH, the increment in the molecular weight of the dendrimer would correspond to the incorporation of the ε-caprolactone monomers. Considering this, the content of PCL was estimated by the difference between the molecular weight of PAMAM-PCL and the PAMAM-OH precursor. The $\overline{M}_n$, the content of ε-caprolactone, the polydispersity and the yield for each system are also summarized in Table S1†.

FTIR spectra for the PAMAM-PCL dendrimers and their precursors (i.e., PAMAM-OH and PCL) are shown in Fig. S2†. The peaks located approximately at 1100 and 1050 cm^{-1} are attributed to the C—O ester bond due to incorporation of PCL blocks. For both dendrimers, as the content of PCL blocks increases, the intensity of the —OH signal (at approximately 3400 cm^{-1}) changes. This could be evidence that the polymerization of PCL blocks onto the peripheral-OH groups of PAMAM was successfully carried out.

3.2. Interfacial tension measurements at the toluene-water and toluene-$AuCl_4^-$ solution interfaces

To gain a better understanding of the behavior of PAMAM-PCL dendrimers at the toluene-water and toluene-$AuCl_4^-$ aqueous solution interfaces, the variation of the interfacial tension, γ, as a function of PAMAM-PCL concentration in toluene solutions, was studied at different temperatures (Fig. 1a). As seen for all samples at both interfaces, in the diluted regime, γ decreases as the PAMAM-PCL concentration increases up to the interfacial tension remains practically unchanged. It is important to mention that at high concentrations of PAMAM-OH at the toluene-water and toluene-$AuCl_4^-$ aqueous solution interfaces, a significant decrease (<1.2 mN/m) in the interfacial tensions was not observed. For the toluene-water interface, the obtained isotherms were shown to depend on the temperature at which the experiments were performed. Increasing the temperature produced a decrease in the interfacial tension, which was attributed to an enhancement of the ability of the interface to solvate the dendrimers. At low temperatures, G4LPCL exhibited a more remarkable decrease in interfacial tension than G4HPCL at similar concentrations. Thus, the interfacial behavior depends on the temperature, amphiphilic character, hydrophilic-hydrophobic balance and the degree of solvation of the dendrimer in the bulk phase. In addition, the hydrophilic character of the PAMAM core contributes to the migration of the dendrimers from the toluene bulk phase to the toluene-water interface. Therefore, toluene would tend to solvate PCL chains, whereas the PAMAM core would be exposed towards the water phase. On this basis, the interfacial activity of G4HPCL is smaller than for G4LPCL because the former would be more solvated in the toluene bulk phase. In the case of the toluene-$AuCl_4^-$ solution interface, the temperature variation showed a similar trend to those observed when the pure water phase was used. The G4LPCL isotherms at the toluene-$AuCl_4^-$ interface displayed a slightly larger decrease in the interfacial tension than the same dendrimer at the toluene-water interface. It is likely that the presence of gold ions in the aqueous phase promotes an increase in the interfacial activity of the G4LPCL dendrimer due to the interactions of the dendrimer-gold ions. At an early stage of the process, the coordination between the carbonyl groups of PCL and $AuCl_4^-$ would take place, generating a change in the conformation of dendrimers, unlike when pure water is used as the phase. In contrast, the behavior of G4HPCL isotherms showed no significant differences in its activity at both interfaces. As mentioned, the interfacial activity of G4HPCL is lower since it would be preferentially solvated by toluene molecules, limiting the possible interactions with the gold ions present in the aqueous phase.The adsorption process of the G4LPCL and G4HPCL dendrimers at the different interfaces was assessed by the Gibbs equation:

$$\Gamma = -(RT)^{-1} C_{PAMAM\text{-}PCL}(d\gamma/dC_{PAMAM\text{-}PCL}) \tag{2}$$

where Γ is the excess interfacial concentration, R is the gas constant and T is the temperature. In addition, the assessment of the slopes, $d\gamma/dC_{PAMAM\text{-}PCL}$, was carried out from the experimental data of γ versus $C_{PAMAM\text{-}PCL}$, which were adjusted to the empirical equation of Szyszkowski:

$$\gamma = \gamma^0 - \gamma B \ \log\left[\left(\frac{C_{PAMAM\text{-}PCL}}{A}\right) + 1\right] \tag{3}$$

where γ^0 is the interfacial tension between the pure phases and A and B are two numerically empirical fitting parameters obtained by iteration. The differentiation of Eq. (3) gives:

$$(d\gamma/dC_{PAMAM\text{-}PCL}) = -\gamma^0 B/(C_{PAMAM\text{-}PCL} + A) \tag{4}$$

Substituting into Eq. (2), the Gibbs–Szyskowski equation then becomes:

$$\Gamma = \gamma^0 B C_{PAMAM\text{-}PCL}/[RT(C_{PAMAM\text{-}PCL} + A)] \tag{5}$$

Using Eq. (5), the dependence of Γ as a function of PAMAM-PCL concentration was studied for these systems. At low dendrimer concentrations, Γ vs $C_{PAMAM\text{-}PCL}$ is almost a linear relationship, while at high concentrations, Γ is practically independent of. Therefore, at $C_{PAMAM\text{-}PCL} \gg$ A:

$$\Gamma^{\infty} = \gamma^0 B/RT \tag{6}$$

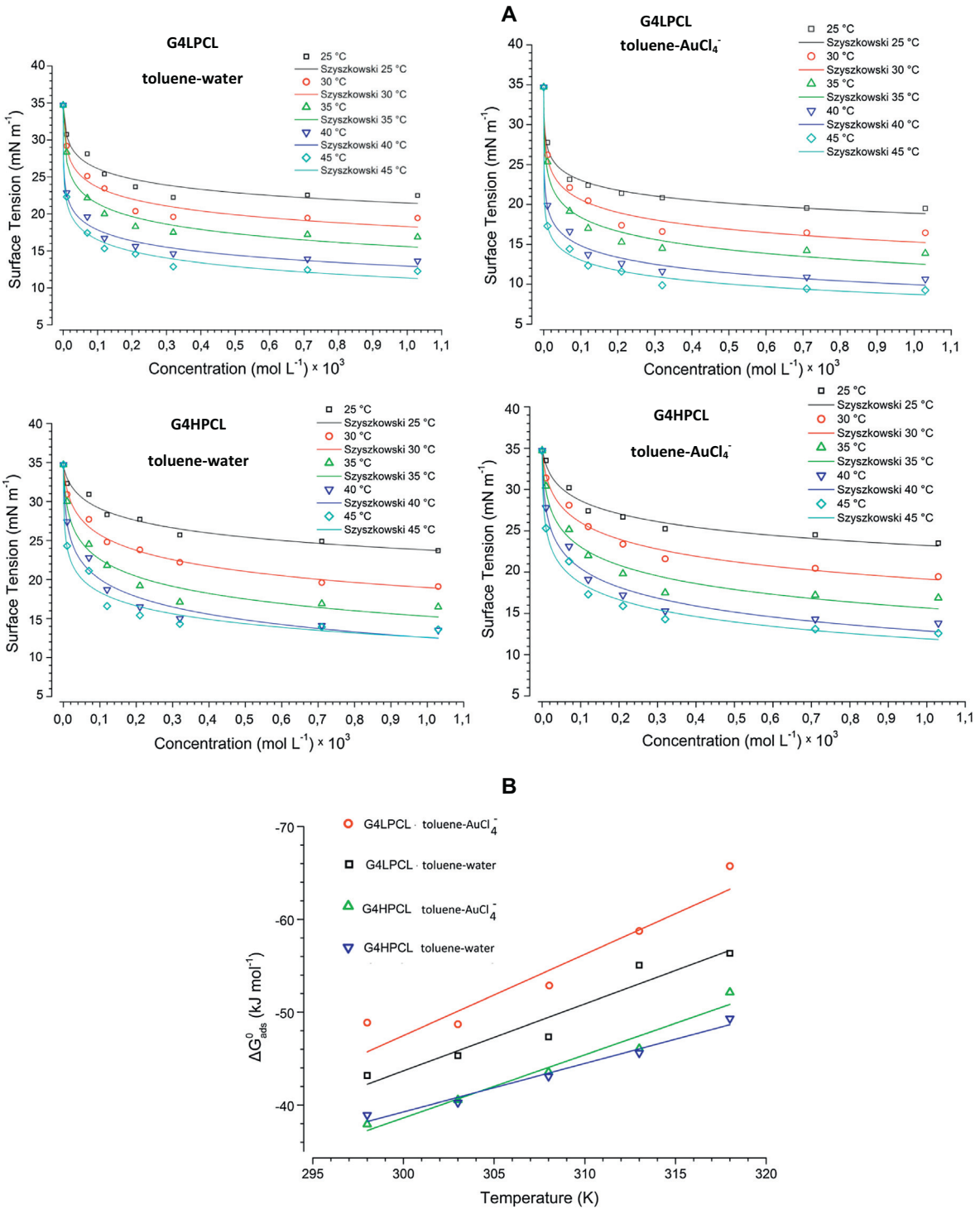

Fig. 1. (a) Interfacial tension as a function of PAMAM-PCL concentration at the respective interfaces and at different temperatures. (b) Standard free energies of adsorption as a function of temperature for G4LPCL and G4HPCL for each interface.

where Γ^{∞} is the limiting excess interfacial concentration. The Γ^{∞} value is related to the average area covered per molecule, σ, according to:

$$\sigma = (\Gamma^{\infty} N_A)^{-1} \tag{7}$$

where N_A is the Avogadro constant. The values of A, B and the respective error from the fitting of Eq. (3) for the G4LPCL and G4HPCL dendrimers at both interfaces are summarized in Table S2.

The σ values for the dendrimers are larger than the values reported for surfactant molecules. These results are expected because surfactants have a well-known structure made up of a hydrophilic head and a hydrophobic tail markedly oriented towards the water and toluene phases, respectively, covering a small interfacial area, whereas the globular shape of the dendrimers should cover a larger average area. Moreover, previous reports have proposed that the average area occupied by the dendrimers would be larger than predicted for the spherical model because dendrimers could adopt an oblate or prolate conformation when confined at the interface. At higher temperatures, the area covered by the dendrimers tends to be smaller than at low temperatures. Apparently, as the temperature increases, the solubility of the dendrimers in the toluene phase increases.

Additionally, in the range of temperatures studied, G4HPCL exhibited smaller σ values compared with G4PCL, evidencing its higher solubility in toluene because it contains a larger amount of PCL. As a result, G4HPCL dendrimers would have a more packed and rigid structure at the interface. In general, the values of σ obtained from G4LPCL isotherms measured at the toluene-$AuCl_4^-$ solution interface are higher compared with those obtained from the toluene-water interface measurements. Considering this, the G4PCL-$AuCl_4^-$interactions promote the interfacial activity of the dendrimer due to a slight increase in the separation of hydrophilic and hydrophobic domains and more expanded structures. In the case of G4HPCL, remarkable differences of σ values obtained for both interfaces were not detected. The preferential solvation of G4HPCL by the toluene phase would be predominant over the interactions with $AuCl_4^-$. For these reasons, a significant similitude in the behavior of G4HPCL at both interfaces is noted, as described above.

3.3. Thermodynamic parameters for the adsorption process

The standard free energies of adsorption, ΔG^0_{ads}, for the adsorption processes of the dendrimers were determined using:

$$\Delta G^0_{ads} = 2.303RT(\log A - 1.74) \tag{8}$$

where A is the parameter mentioned above. The obtained values of ΔG^0_{ads} are listed in Table S3†. As interpreted from the negative values of the standard free energy of adsorption, ΔG^0_{ads}, the adsorption process takes place spontaneously in all cases. The ΔG^0_{ads} values become more negative for dendrimers as the temperature increases. These values help corroborate the possible effect of the temperature on the conformation and ordering of the dendrimer at the interface. Alternatively, the mathematical expression of the standard adsorption entropy is as follows:

$$-\Delta S^0_{ads} = \frac{d\Delta G^0_{ads}}{dT} \tag{9}$$

To evaluate the standard entropy of the adsorption process, ΔS^0_{ads}, the dependence of ΔG^0_{ads} on temperature was plotted (Fig. 1b). For these calculations, ΔS^0_{ads} was considered constant over the range of temperatures studied here. From the slopes of these curves, the ΔS^0_{ads} values were obtained. The values were found to be slightly negative for both dendrimers at both interfaces. The adsorbed G4LPCL and G4HPCL dendrimers at the toluene-water (or $AuCl_4^-$ solution) interface should adopt a conformation more ordered than that in the bulk solution. The standard enthalpy of the adsorption process, ΔH^0_{ads}, was estimated according to the following equation:

$$\Delta H^0_{ads} = -T^2 \frac{d\left(\frac{\Delta G^0_{ads}}{T}\right)}{dT} \tag{10}$$

In this case, the ΔH^0_{ads} values were more negative. The values of thermodynamic parameters for the interfacial activity of the dendrimers are listed in Table S3†. Thereby, small negative values for ΔS^0 and larger negative values for ΔH^0 were found for the adsorption process of the dendrimers, suggesting that the adsorption process is enthalpy-driven. The energy associated in the adsorption process of PAMAM-PCL dendrimers could be explained in terms of a balance between two competing effects: (i) the desolvation of the toluene molecules of the PCL chains (endothermic process) and (ii) a certain degree of solvation of the PAMAM core by water molecules (exothermic process). Thus, the adsorption process of the G4HPCL would involve higher desolvation energies of toluene molecules due to its larger PCL chains. Specifically, the energy involved in the G4LPCL desolvation process should be smaller than in the G4HPCL case. On this basis, at the interface, G4LPCL could preserve a similar conformation to that adopted in bulk toluene. This behavior is corroborated by the higher average areas covered by the G4LPCL dendrimers. Therefore, a relatively lower energy is needed for the process of toluene desolvation and further solvation by water molecules for G4LPCL in comparison with the case of G4HPCL. Because of this, in the range of temperatures analyzed, G4HPCL presents lower negative ΔH^0_{ads} values than G4LPCL at both interfaces.

3.4. Surface activity measurements at the air-water interface

A study of the ability of PAMAM-PCL dendrimers to form monolayers at the air–water interface with and without $AuCl_4^-$ present in the subphase, at different temperatures, by compression using the Langmuir technique, was performed. The spreading solvent used in all cases was chloroform. The surface pressure (π) as a function of area per repeating unit (A) isotherms obtained for the PAMAM-PCL dendrimers at both interfaces and at three temperatures (25, 30 and 35 °C) are shown in Fig. 2. From the isotherms, the gradual increment of π when the monolayer is compressed can be clearly observed. In general for the case of the polymeric system, three different surface concentration regions should be noted, (i) in the dilute regime, 0–0.1 mg m^{-2}, (i.e. a pseudo gas state) πincrements gradually occur when the monolayer is compressed, (ii) in the semi-dilute regime, 0.1–1 mg m^{-2}, (i.e. pseudo liquid state) πincrements sharply occur due to the monolayer compression and iii) in the concentrated regime, >1 mg m^{-2}, (i.e. pseudo solid state) π increments occur slowly again to reach the pressure of the collapse of the monolayer.

It is possible to distinguish that the G4LPCL isotherms are of the expanded type and the G4HPCL ones are of the condensed type, because there is a larger affinity between G4LPCL and the interface than G4HPCL. In general, G4LPCL exhibits higher surface pressure values compared with G4HPCL, at a constant value of area. This helps to confirm that the PCL of G4LPCL chains would be more expanded at the interface. In addition, notorious differences in the obtained isotherms according to the subphase used were detected, reflecting the possible existence of dendrimer-$AuCl_4^-$ interactions. To gain insights about these different behaviors, the static elasticity modulus, ε_0, was obtained from π vs A isotherms, according to the equation:

$$\varepsilon_0 = \frac{d\gamma}{d\ln A} \tag{11}$$

where γ is the difference between the surface tension of pure water (72.1 mN m^{-1}) and the surface pressure, π.

The ε_0 dependence on π for the samples of PAMAM-PCL monolayers at both interfaces and at different temperatures is also shown in Fig. 2 (insets). In general, the elasticity maximum is found to be in the semi-dilute region for polymeric monolayers. The more remarkable changes of ε_0 were found to be ranged between 3.0 and 4.5 mN m^{-1} of surface pressure. At higher values than 4.8 mN m^{-1}, a notorious decrease in the elasticity for all samples was observed at the air-water interface. An important aspect is the determination of the collapse pressure (π_c) for the monolayers which remains not entirely elucidated until now. A generally accepted criterion to estimate the π_c would be from the elasticity curves as a function of the

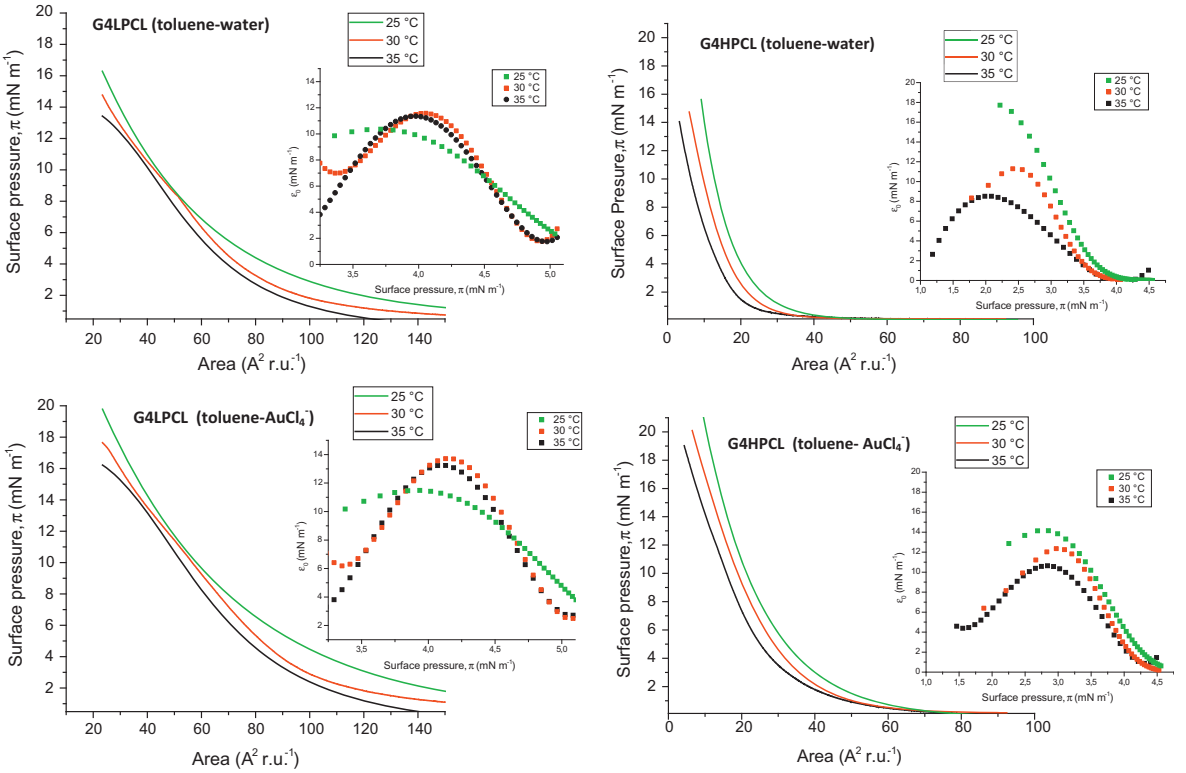

Fig. 2. Surface pressure–area isotherms for PAMAM-PCL dendrimers at different temperatures for each interface. The insets correspond to the static elasticity modulus as a function of the surface pressure.

surface pressure. Thereby, the π_c is assigned to the value of surface pressure at which the surface pressure initiates to grow upon reaching the minimum value of ε_0 (i.e. the higher degree of packaging of the monolayers). The collapse pressure for all samples is summarized in Table S4a†. It is important to note that the collapse pressure could not be determined unequivocally for the isotherms at 25 °C. However, the π_c of the monolayers at low temperatures should be higher than those obtained at higher temperatures. In addition, when $AuCl_4^-$ was used as the subphase, a different behavior of the elasticity was detected. The maximum of ε_0 was shifted toward lower values of surface pressures. These shifts become more remarkable as the temperature increased. This could be attributed to the interactions between $AuCl_4^-$ and the PAMAM-PCL monolayer which appear to be more favored at higher temperatures. Moreover, for the $AuCl_4^-$ subphase, the surface pressures associated with the maximum values of ε_0 for both dendrimers at the interval of temperatures studied, were smaller compared with pure water confirming that the surface activity of dendrimers is affected due to the presence of $AuCl_4^-$ in the subphase.

Alternatively, the scaling concepts of the behavior of PAMAM-PCL monolayers formed in the semi-dilute regime could be explained with some degree of accuracy. The relationship between the surface pressure and the surface concentration in this regime is as follows:

$$\pi = \Gamma^{2\nu/(2\nu-1)} \tag{12}$$

where Γ is the surface concentration in mg m^{-2} and ν is the critical exponent of the excluded volume, which is related to the thermodynamic quality of the interface as a bi-dimensional pseudo solvent for the monolayers. In the semi-dilute regime, a $\mathrm{Log}\,\pi$ vs $\mathrm{Log}\,\Gamma$ plot would yield a linear variation having a slope equal to $2\nu/(2\nu - 1)$. According to the trend of the slopes, the nature of the interactions present and the affinity of the dendrimers for the interface should be reflected. For good solvents (i.e. good thermodynamic quality), ν is close to 0.8, whereas values closer to 0.5 are related with theta solvent conditions. The obtained ν values are listed in Table S4b†. For the G4LPCL and G4HPCL monolayers on the pure water subphase at 25 °C, the ν values are approximately of 0.69 and 0.57, respectively, revealing that the thermodynamics quality air-water interface is better for G4LPCL. At higher temperatures, the values of ν slightly increase for G4HPCL and decrease for G4LPCL, contributing to the enhancement of the hydrophobic character of G4HPCL, orienting it toward the air phase. For the $AuCl_4^-$ solution as the subphase, the ν values of G4LPCL are higher than those obtained for the pure water subphase for all temperatures. It is likely that the formed monolayers would have a larger affinity for the air-$AuCl_4^-$ solution interface in the semi-diluted regime, caused by the presence of ionic species in the subphase.

3.5. Formation of gold nanoparticles at the toluene-$AuCl_4^-$ solution and air-$AuCl_4^-$ solution interfaces

The behavior of the interfacial activity of the PAMAM-PCL dendrimers reflected some kind of interactions with $AuCl_4^-$ at the toluene-$AuCl_4^-$ solution interface. However, these results would not be sufficient to clarify the possible formation of gold nanoparticles. Therefore, UV–vis spectroscopy and AFM techniques were used to verify the possible presence of gold nanoparticles. UV–vis spectra (Fig. S3†) show the obtained gold nanoparticles using a concentration of dendrimer of 0.21 mol $L^{-1} \times 10^3$ at different times of immersion of the $AuCl_4^-$ solution drop into the toluene solution of dendrimers. After 15 min reaction time, it is observed the apparition of typical maximum of absorption band due to the presence of the gold nanoparticles located approximately at 550 and 580 nm for G4LPCL and G4HPCL, respectively. As the reaction time takes place the band absorption increases. Additionally, this absorption band is shifted toward lower wavenumbers due to the formation of a larger amount of nanoparticles and a possible change in the size or aggregation of gold nanoparticles. After 1 h of reaction, there was no a significant increasing in the absorption band of gold nanoparticles. AFM images of neat films of dendrimers and gold nanoparticles synthesized with both dendrimers (after 1 h reaction time) were obtained onto silicon wafer upon evaporation of the mixed toluene-water solvents under vacuum at room temperature (Fig. 3a). From these images (Fig. 3a, insets) it is possible to distinguish the differences of surface-roughness profiles between PAMAM-PCL films obtained from toluene-water and toluene-$AuCl_4^-$ solution interfaces. Table S5† summarizes the values of root mean square roughness (RMSr) for PAMAM-PCL at both interfaces. Higher roughness values were obtained for both G4LPCL and G4HPCL films obtained from toluene-$AuCl_4^-$ solution which could be attributed to the presence of gold nanoparticles embedded into dendrimer monolayer. The estimated sizes by AFM topographic profiles of gold nanoparticles are listed in Table S6†.

Similarly, as described above, the formation of gold nanoparticles at the air-$AuCl_4^-$ solution interface was also evidenced by the same techniques used for the pendant drop experiments. Fig. S3b† shows the UV–vis spectra obtained when we used the $AuCl_4^-$ solution subphase. The spectra were recorded at different reaction times maintaining constant the surface pressure at 4.0 mN m^{-1} and 2.5 mN m^{-1} for G4LPCL and G4HPCL, respectively. These surface pressures were chosen in order to ensure a regimen of concentration slightly below the maximum of elasticity. The band maxima were located approximately at 560 and 570 nm for G4LPCL and G4HPCL, respectively. The absorption increased significantly during 1 h of reaction indicating the formation of a larger amount of nanoparticles. AFM images obtained after 1 h of the reaction time at 25 °C are also shown in Fig. 3b. Just as toluene-$AuCl_4^-$ interface, topographic changes are observed when we varied the subphase from water to $AuCl_4^-$ solution (Fig. 3b, insets). The RMSr resulted to be higher for PAMAM-PCL films obtained formed at the air-$AuCl_4^-$ solution interface than those formed at the air-water interface (Table S5†). These differences in the monolayer topography are also evidenced according to the dendrimer used. Therefore, the interface and the type of dendrimer present at the interface would influence the morphological and size of the obtained PAMAM-PCL-gold nanoparticle monolayers. In this case, the gold nanoparticles obtained from air-$AuCl_4^-$ were smaller in size compared with those formed at the

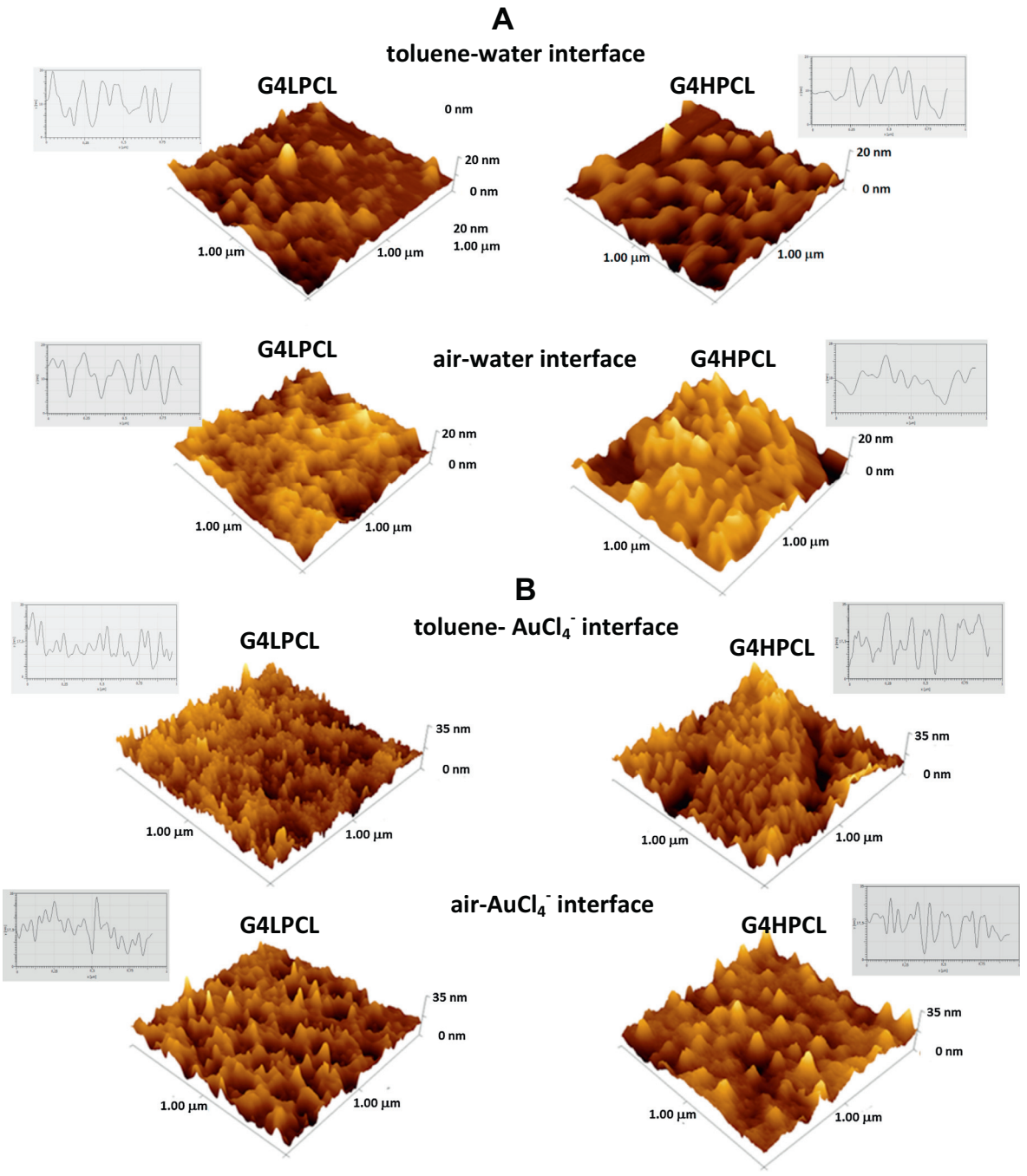

Fig. 3. AFM images obtained for GL4PCL and G4HPCL dendrimers and the respective obtained gold nanoparticles at the (a) toluene-water and air-water interfaces and at the (b) toluene-$AuCl_4^-$ and air-$AuCl_4^-$ interfaces. The topographies of dendrimers and gold nanoparticles correspond to 1 h after deposition of monolayers at 298 K. The insets correspond to surface-roughness profiles for each sample.

toluene-$AuCl_4^-$ interface. It is likely that at the air-$AuCl_4^-$, the dendrimer monolayers have more exposed their functional groups toward aqueous subphase favoring the nucleation and growth processes to form gold nanoparticles.

In previous studies, we have demonstrated that noble metal ion reduction can be performed by a variety of homopolymers and copolymers containing hydroxyl end groups [82,83]. In this case, the role of the reduction process is assigned to the hydroxyl end groups of PAMAM-PCL dendrimers. This reaction should be promoted when hydroxyl end groups of dendrimers forming the monolayer are found to be oriented toward the $AuCl_4^-$ solution phase, enhancing the dendrimer-$AuCl_4^-$ ions contact sites.

Therefore, the hydroxyl end groups should contribute heavily to the reducing power of these dendrimers. A proposed mechanism for the reduction of gold ions is as follows:

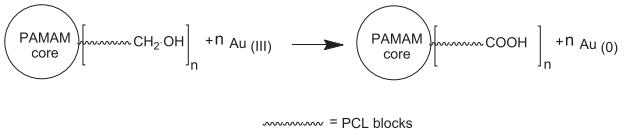

According to this mechanism, the redox reaction could produce the oxidized form of a hydroxyl end group (i.e., a carboxylic acid group) and metal atoms. In addition, a schematic representation of these reactions and possible interactions as well as further formation of gold nanoparticles at both interfaces is depicted in Scheme 1.

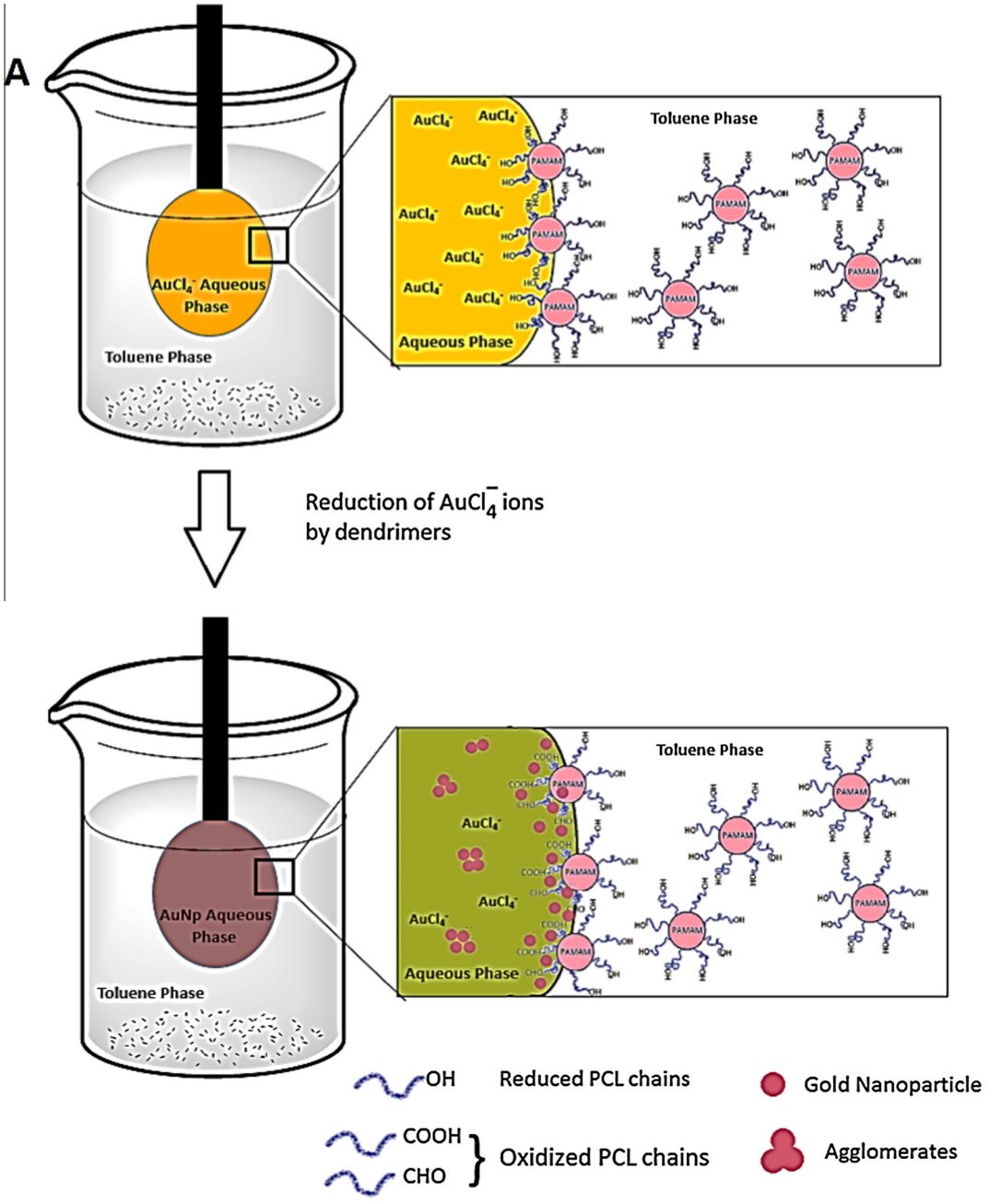

Scheme 1. Illustration of the synthesis of gold nanoparticles with PAMAM-PCL dendrimers at the (a) toluene-$AuCl_4^-$ solution and (b) air-$AuCl_4^-$ solution interfaces.

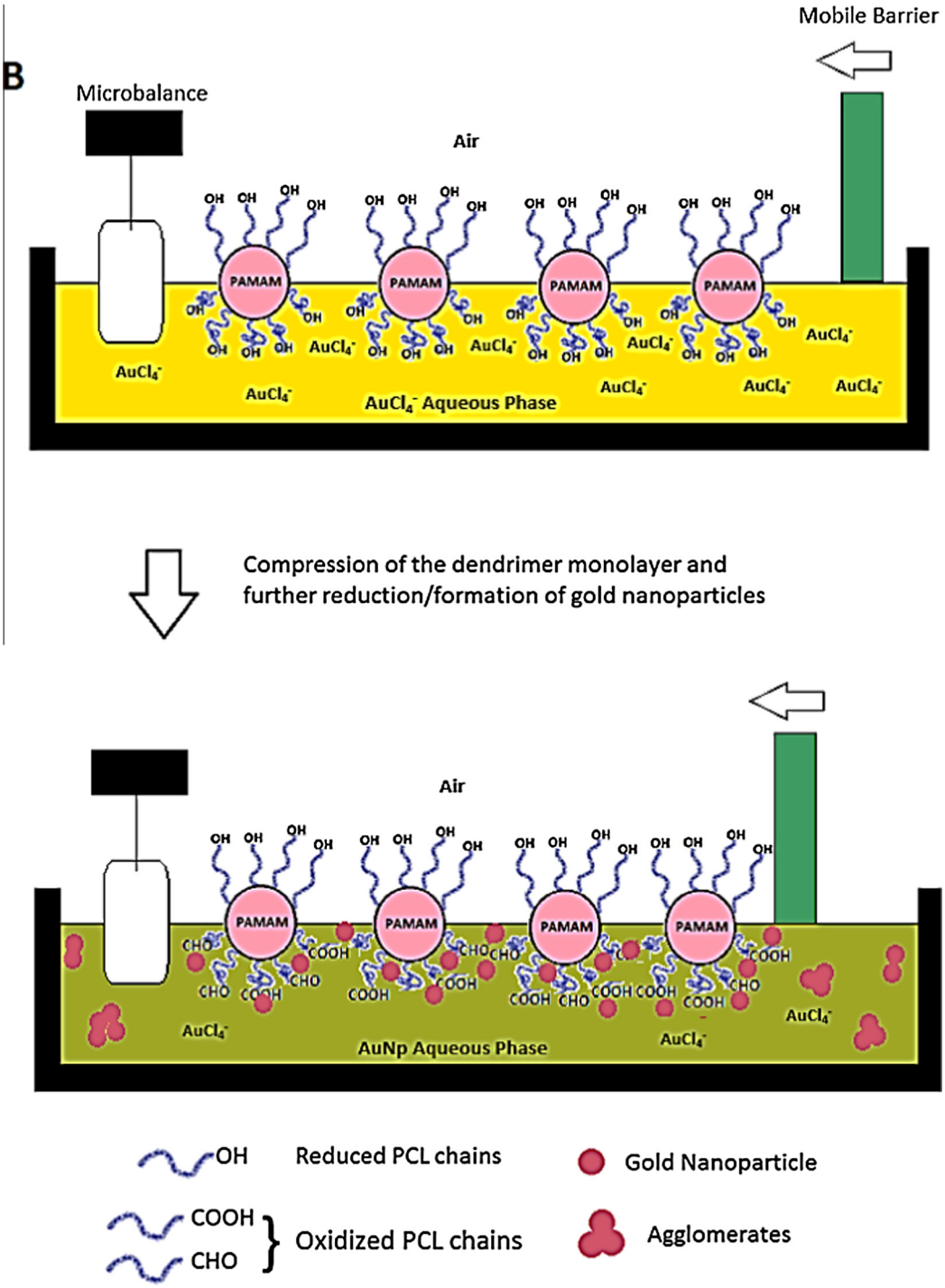

Scheme 1 (*continued*)

3.6. Molecular simulation and electronic structure calculations

It is likely that the most striking features of the interfacial activity of dendrimers are a result of their geometrical and spatial arrangements. In order to address this matter, a comparative visual approach between the trajectories of the PAMAM-OH and PAMAM-PCL systems at the toluene-water interface are shown in Fig. 4a. This interface was chosen to be simulated due to the possible interpretation at molecular level of thermodynamic parameters obtained from pendant drop experiments.

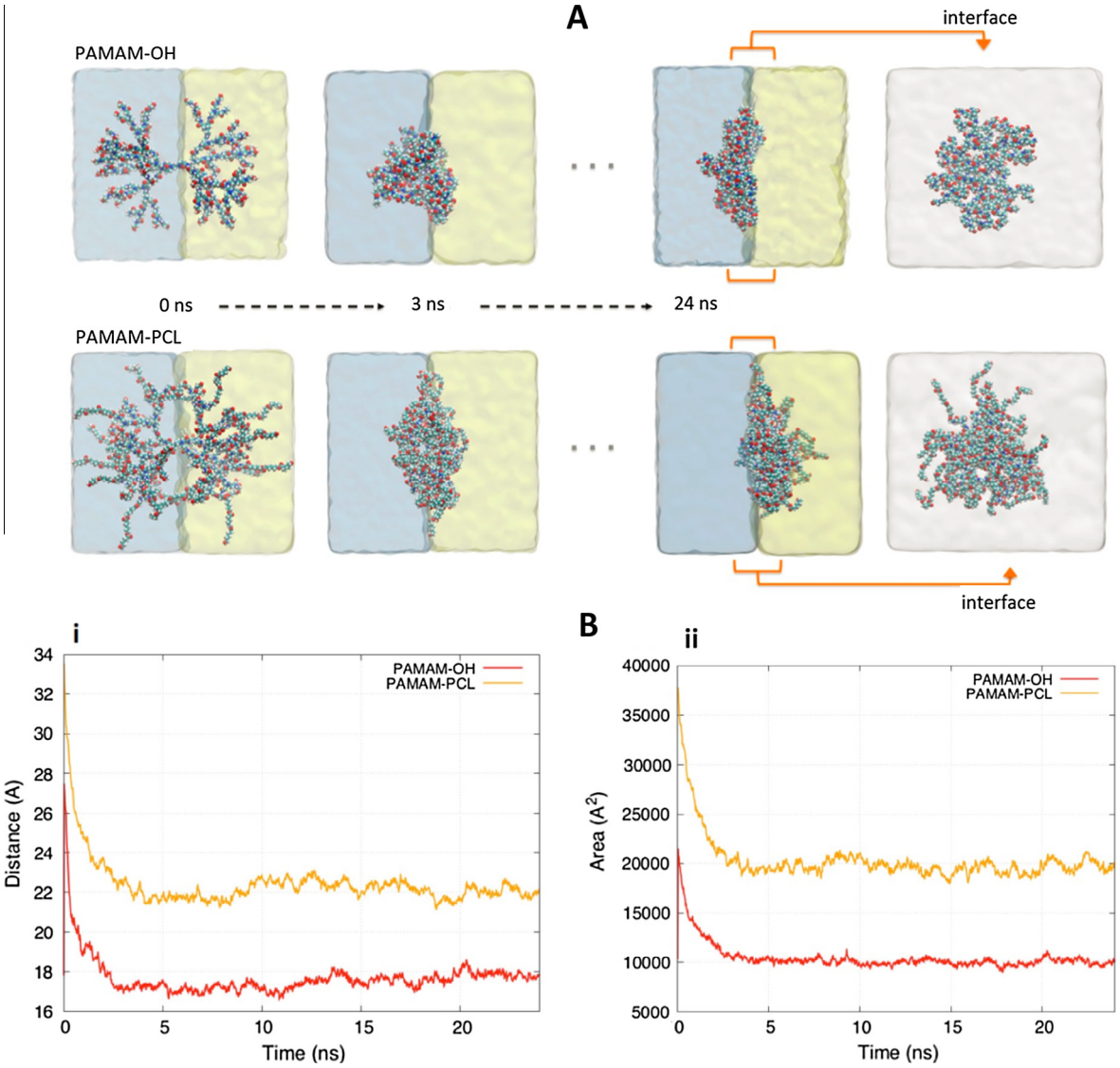

Fig. 4. (a) Snapshots of trajectories for PAMAM-OH and PAMAM-PCL systems at the toluene-water interface (colored as yellow and blue, respectively) at 0.0, 3.0 and 24.0 ns of simulated time. In both cases, the last image represents the dendrimer structure from bottom(toluene phase)-up(water phase) view. (b) Comparative graphs of (i) radius of gyration and (ii) SASA values for PAMAM-OH (yellow lines) and PAMAM-PCL (red lines) trajectories. In both cases, the total simulated time was 24.0 ns. (For interpretation of the references to color in this figure legend, the reader is referred to the web version of this article.)

Both dendrimers modified the structure of their spatial distribution to remain at the interface. Initially, both dendrimers adopt a disk-shaped at the interface, but as time passes, an oval shaped was adopted. In addition, the hydrophilic groups and aliphatic hydrophobic chains tend to interact selectively with water and toluene solvents, respectively. The molecular simulations showed that PAMAM-PCL dendrimer remains at the toluene-water- interface, adapting its molecular conformation to the polar/apolar environment. Thus, in order to gain stability at the interface, PAMAM core and poly(ε-caprolactone) chains would be oriented towards water and toluene phase, respectively. On the other hand, PAMAM-OH remains also at the interface but gradually its hydrophilic groups interact with the water solvent, decreasing dendrimer-toluene phase interaction. These observations are coherent with the significant enthalpic contribution previously described for dendrimers at the toluene-water interface.

According to simulation time, the initial values of radius of gyration were 17.8 and 33.5 Å for PAMAM-OH and PAMAM-PCL, respectively (Fig. 4bi). Then, both curves show a similarly constant decreasing as time elapses: 21.9 and 17.6 Å at 5 ns; 17.1 and 22.8 Å at 10 ns; 17.4 and 22.1 Å at 15 ns; 17.9 and 21.7 Å at 20 ns and 17.8 and 22.1 Å at 24 ns, respectively. Therefore, PAMAM-PCL trajectory exhibited always higher values of radius of gyration than those of PAMAM-OH. This suggests that PAMAM-PCL structure has a lower level of compactness which is attributed to poly(ε-caprolactone) chains and their interaction with the toluene phase increasing the radial dimensions of this system.

A

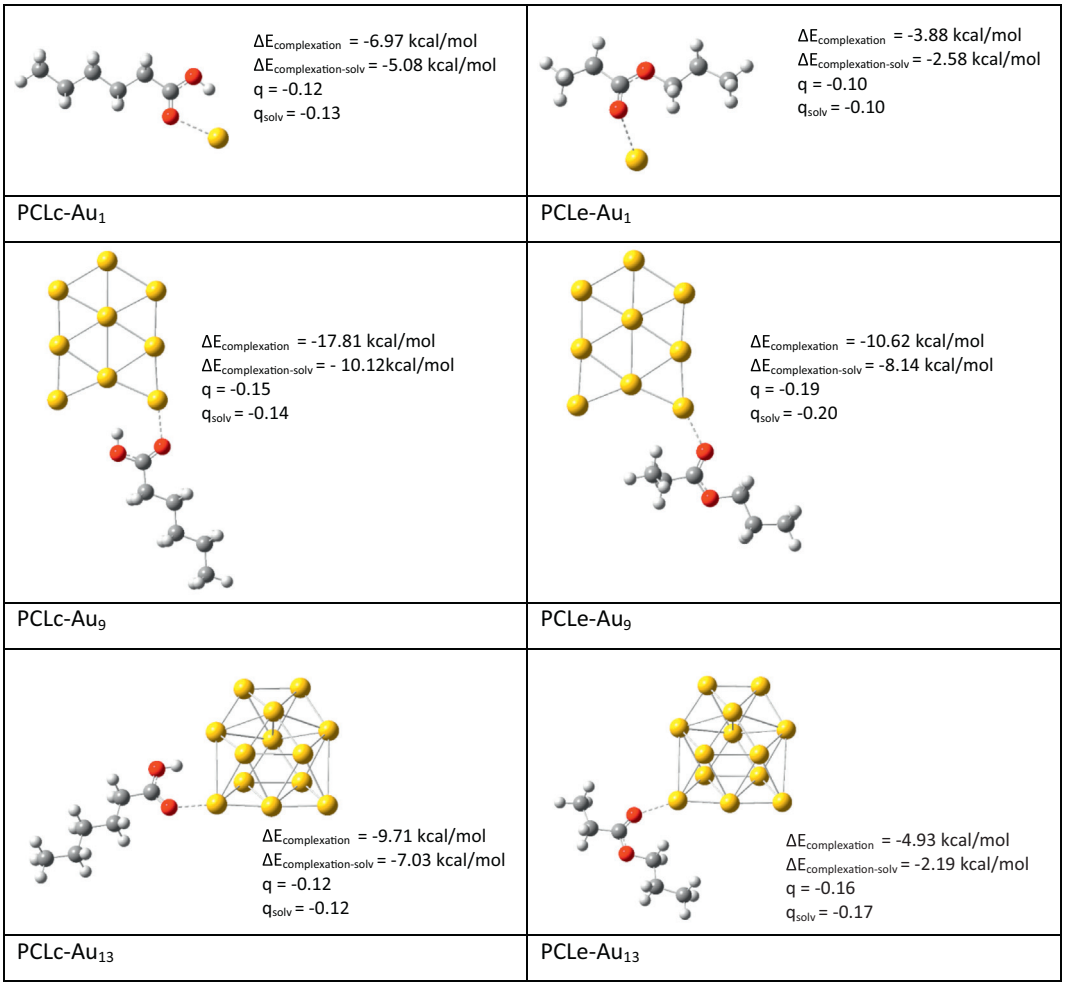

B

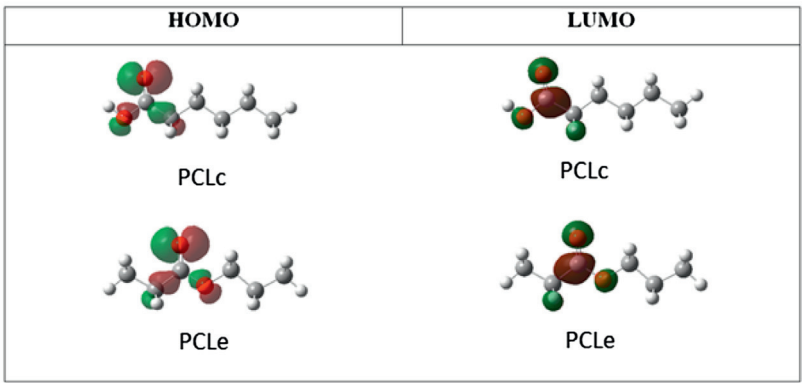

Fig. 5. (a) Most stable complexes of PCLc and PCLe with Au_n clusters. The dashed lines show the closest atoms between PCL monomer and metal cluster. The complexation energies ($\Delta E_{complexation}$) and net charges (q) for the monomer-Au_n complexes and Au_n clusters are also shown. The calculations considering solvent effects are referred as $\Delta E_{complexation\text{-}solv}$ and q_{solv}. (b) Canonical representation of the frontier orbitals HOMO-LUMO for each structure of PCLc and PCLe.

The SASA analyses shown in Fig. 4bii exhibit a similar trend that radius of gyration. PAMAM-PCL has higher values of SASA than those of the PAMAM-OH system. The initial values were 37,736 and 10,333 $Å^2$, for PAMAM-PCL and PAMAM-OH, respectively. After 5.0 ns of simulation time, these values decreased by approximately 20,000 $Å^2$ for PAMAM-PCL and 10,000 $Å^2$ for PAMAM-OH. At 24 ns, the areas were 19,544 and 10,296 A^2 for PAMAM-PCL and PAMAM-OH, respectively. As expected, poly(ε-caprolactone) chains contribute to increasing the total area of PAMAM-PCL dendrimer at the interface. Additionally, PAMAM-OH shows a more uniform curve compared to PAMAM-PCL which displays several peaks and pits due to a larger spatial distribution and degree of freedom of PCL chains.

Additionally, to provide a better understanding of the interactions between PCL and gold nanoparticles, computational electronic structure calculations were carried out. For this, under vacuum and PCM model calculations were performed. Two monomer models, PCLc and PCLe (where c = carboxylic acid group or x = ester group) and Au_n (n = 1, 9 and 13) clusters were designed. Fig. 5a shows the most stable structure for each monomer-Au_n complex. Under vacuum calculations, the formation of the PCL-Au_n complex should mainly be guided by interactions of the carbonylic oxygen over external Au atoms located at the border of clusters [84,85]. Moreover, the results of the interactions for PCL-Au_n complexes established that the geometry of gold clusters remains almost unchanged.

Complexation energies for all studied monomer-Au_n systems and the net charges (computed as the sum over all gold atoms) on Au_n clusters in the complexes were calculated (Fig. 5a). These calculations showed that PCLc-Au_n complexes resulted to be energetically more stable than PCLe-Au_n ones. Apparently, the formation of complexes is increased by carbonylic oxygen-Au_n cluster interactions. This is supported by the frontier orbitals analysis of the PCL monomers, in which spatial distribution of HOMO and LUMO are very similar for both structures (Fig. 5b). The charge analysis of clusters showed an electronic transfer from carbonylic oxygen to Au_n clusters which would indicate the type of interactions in these systems. It is likely that the PCL chains could adapt their geometry in order to optimize multiple interactions with gold nanoparticles. Alternatively, when incorporating water as an implicit solvent, the complexation energies and charges of Au clusters are attenuated but maintained the same trends as described above [83].

4. Conclusions

The obtained results showed that the adsorption process at the toluene-water interface depends strongly on the hydrophilic–hydrophobic balance between the PAMAM and PCL chains present in the dendrimeric structure. Specifically, the interfacial activity was higher for the G4LPCL dendrimer at the interval of temperatures assayed. In addition, the presence of gold ions in the aqueous phase increased the interfacial activity for the G4LPCL dendrimer. This was attributed to significant interactions between the dendrimer and $AuCl_4^-$ ions. In the case of G4HPCL, the isotherms obtained at both the toluene-water and the toluene-$AuCl_4^-$ interfaces were relatively similar to each other, evidencing that the interactions with $AuCl_4^-$ ions should be more restricted in comparison with the case of G4LPCL. For the studies performed at the air-water interface, the G4LPCL and G4HPCL isotherms shown to be of the type expanded and condensed, respectively. Similarly, differences in the obtained isotherms at the air-water and air-$AuCl_4^-$ solution interfaces are also attributed to the dendrimer-$AuCl_4^-$ ions interactions.

In addition, the formation of gold nanoparticles studied having $AuCl_4^-$ solution as a phase was evidenced using UV–vis and AFM techniques. The topography of the samples was shown to be dependent mainly on the types of interface and dendrimers used, as well as the presence of gold nanoparticles.

Molecular dynamics simulations were shown to be a very useful tool to gain a better understanding of the stability and tri-dimensional arrangement of dendrimers at the toluene-water interface. These studies allowed to obtain information on the conformational change and spatial distribution of PAMAM-OH and PAMAM-PCL dendrimers.

Theoretical quantum analyses allowed to explain the possible interactions between PCL monomers with uni-, bi- and tri-dimensional gold clusters. In this case, the O-Au interaction would drive the formation of PCL-Au_n complexes. These interactions resulted to be stronger for PCL having carboxylic acid end groups.

Finally, the study and characterization of the possible catalytic activity of these dendrimeric systems with gold nanoparticles is currently in progress. The above aimed to provide novel alternatives for potential technological applications, including biological interfaces, membranes, photovoltaic cells and hydrogen evolution.

Acknowledgment

C.S. and M.M.-L. thank to Post-doctoral Fondecyt grant 3140385 and 3150544, respectively. A.P.M., A.R. and F.A.-S., thank for doctoral scholarships to CONICYT-PCHA/Doctorado Nacional 2016-21161314, 2016-21161240 and 2013-21130308, respectively.

Appendix A. Supplementary material

Supplementary data associated with this article can be found, in the online version, at http://dx.doi.org/10.1016/j.eurpolymj.2016.09.017.

References

[1] R. Duro, C. Souto, J. Gomez-Amoza, R. Martinez-Pacheco, A. Concheiro, Interfacial adsorption of polymers and surfactants: implications for the properties of disperse systems of pharmaceutical interest, Drug Develop. Ind. Pharm. 25 (7) (1999) 817–829.
[2] F.O. Opawale, D.J. Burgess, Influence of interfacial properties of lipophilic surfactants on water-in-oil emulsion stability, J. Colloid Interface Sci. 197 (1) (1998) 142–150.
[3] S. Rouimi, C. Schorsch, C. Valentini, S. Vaslin, Foam stability and interfacial properties of milk protein–surfactant systems, Food Hydrocolloids 19 (3) (2005) 467–478.
[4] J.B. Massey, H.S. She, H.J. Pownall, Interfacial properties of model membranes and plasma lipoproteins containing ether lipids, Biochemistry 24 (24) (1985) 6973–6978.
[5] D. Kitamoto, H. Isoda, T. Nakahara, Functions and potential applications of glycolipid biosurfactants—from energy-saving materials to gene delivery carriers—, J. Biosci. Bioeng. 94 (3) (2002) 187–201.
[6] B.-H. Jeong, E.M. Hoek, Y. Yan, A. Subramani, X. Huang, G. Hurwitz, A.K. Ghosh, A. Jawor, Interfacial polymerization of thin film nanocomposites: a new concept for reverse osmosis membranes, J. Membr. Sci. 294 (1) (2007) 1–7.
[7] S.H. Anastasiadis, I. Gancarz, J.T. Koberstein, Compatibilizing effect of block copolymers added to the polymer/polymer interface, Macromolecules 22 (3) (1989) 1449–1453.
[8] B.J. Kim, S. Given-Beck, J. Bang, C.J. Hawker, E.J. Kramer, Importance of end-group structure in controlling the interfacial activity of polymer-coated nanoparticles, Macromolecules 40 (6) (2007) 1796–1798.
[9] R. Agrawal, G. Pandey, Solid polymer electrolytes: materials designing and all-solid-state battery applications: an overview, J. Phys. D: Appl. Phys. 41 (22) (2008) 223001.
[10] S. Zeppieri, J. Rodríguez, A. López de Ramos, Interfacial tension of alkane + water systems, J. Chem. Eng. Data 46 (5) (2001) 1086–1088.
[11] N.P. Ashby, B.P. Binks, V.N. Paunov, Formation of giant colloidosomes by transfer of pendant water drops coated with latex particles through an oil–water interface, Phys. Chem. Chem. Phys. 6 (17) (2004) 4223–4225.
[12] A. Ulman, An Introduction to Ultrathin Organic Films: From Langmuir-Blodgett to Self-Assembly, Academic Press, 2013.
[13] E.Y. Lee, M.P. Suh, A robust porous material constructed of linear coordination polymer chains: reversible single-crystal to single-crystal transformations upon dehydration and rehydration, Angew. Chem. 116 (21) (2004) 2858–2861.
[14] N. Reitzel, D.R. Greve, K. Kjaer, P.B. Howes, M. Jayaraman, S. Savoy, R.D. McCullough, J.T. McDevitt, T. Bjørnholm, Self-assembly of conjugated polymers at the air/water interface. Structure and properties of Langmuir and Langmuir-Blodgett films of amphiphilic regioregular polythiophenes, J. Am. Chem. Soc. 122 (24) (2000) 5788–5800.
[15] J. Maldonado-Valderrama, H. Wege, M. Rodriguez-Valverde, M. Galvez-Ruiz, M. Cabrerizo-Vilchez, Comparative study of adsorbed and spread β-casein monolayers at the water-air interface with the pendant drop technique, Langmuir 19 (20) (2003) 8436–8442.
[16] R. Good, Surface and Colloid Science: Volume 11: Experimental Methods, Springer Science & Business Media, 2012.
[17] S.A. Gundersen, M.-H. Ese, J. Sjöblom, Langmuir surface and interface films of lignosulfonates and kraft lignins in the presence of electrolyte and asphaltenes: correlation to emulsion stability, Colloids Surf. A: Physicochem. Eng. Aspects 182 (1) (2001) 199–218.
[18] Ø. Brandal, J. Sjöblom, Interfacial behavior of naphthenic acids and multivalent cations in systems with oil and water. II: Formation and stability of metal naphthenate films at oil-water interfaces, J. Dispers. Sci. Technol. 26 (1) (2005) 53–58.
[19] V. Ganesan, C.J. Ellison, V. Pryamitsyn, Mean-field models of structure and dispersion of polymer-nanoparticle mixtures, Soft Matter 6 (17) (2010) 4010–4025.
[20] K.T. Tallakstad, H.A. Knudsen, T. Ramstad, G. Løvoll, K.J. Måløy, R. Toussaint, E.G. Flekkøy, Steady-state two-phase flow in porous media: statistics and transport properties, Phys. Rev. Lett. 102 (7) (2009) 074502.
[21] M. Maccarini, R. Steitz, M. Himmelhaus, J. Fick, S. Tatur, M. Wolff, M. Grunze, J. Janecek, R. Netz, Density depletion at solid-liquid interfaces: a neutron reflectivity study, Langmuir 23 (2) (2007) 598–608.
[22] X. Zhao, F. Pan, P. Coffey, J.R. Lu, Cationic copolymer-mediated DNA immobilization: interfacial structure and composition as determined by ellipsometry, dual polarization interferometry, and neutron reflection, Langmuir 24 (23) (2008) 13556–13564.
[23] A. Mourran, Y. Wu, R.A. Gumerov, A. Rudov, I.I. Potemkin, A. Pich, M. Möller, When colloidal particles become polymer coils, Langmuir (2015).
[24] Y. Wang, D.K. Sang, Z. Du, C. Zhang, M. Tian, J. Mi, Interfacial structures, surface tensions, and contact angles of diiodomethane on fluorinated polymers, J. Phys. Chem. C 118 (19) (2014) 10143–10152.
[25] L. Yu, P. Zhang, H. Yang, G. Yang, J. Zhang, J. Wang, Aggregation behaviors of novel amphiphilic dendrimers at solid-liquid interface, J. Dispers. Sci. Technol. 35 (3) (2014) 456–462.
[26] M. Stamm, Polymer Surfaces and Interfaces, Polymer Surfaces and Interfaces: Characterization, Modification and Applications, vol. 1, Springer, Berlin Heidelberg, 2008. ISBN 978-3-540-73864-0.
[27] D.S. Katti, R. Vasita, K. Shanmugam, Improved biomaterials for tissue engineering applications: surface modification of polymers, Curr. Top. Med. Chem. 8 (4) (2008) 341–353.
[28] S.K. Hau, H.-L. Yip, O. Acton, N.S. Baek, H. Ma, A.K.-Y. Jen, Interfacial modification to improve inverted polymer solar cells, J. Mater. Chem. 18 (42) (2008) 5113–5119.
[29] S. Svenson, D.A. Tomalia, Dendrimers in biomedical applications—reflections on the field, Adv. Drug Deliv. Rev. 64 (2012) 102–115.
[30] A. Samad, M.I. Alam, K. Saxena, Dendrimers: a class of polymers in the nanotechnology for the delivery of active pharmaceuticals, Curr. Pharm. Des. 15 (25) (2009) 2958–2969.
[31] J. Hu, Y. Cheng, Q. Wu, L. Zhao, T. Xu, Host-Guest chemistry of dendrimer-drug complexes. 2. Effects of molecular properties of guests and surface functionalities of dendrimers, J. Phys. Chem. B 113 (31) (2009) 10650–10659.
[32] J. Hu, T. Xu, Y. Cheng, NMR insights into dendrimer-based host–guest systems, Chem. Rev. 112 (7) (2012) 3856–3891.
[33] J. Satija, V. Sai, S. Mukherji, Dendrimers in biosensors: concept and applications, J. Mater. Chem. 21 (38) (2011) 14367–14386.
[34] D. Astruc, E. Boisselier, C. Ornelas, Dendrimers designed for functions: from physical, photophysical, and supramolecular properties to applications in sensing, catalysis, molecular electronics, photonics, and nanomedicine, Chem. Rev. 110 (4) (2010) 1857–1959.
[35] A. Su, S. Tan, P. Thapa, B.N. Flanders, W.T. Ford, Highly ordered langmuir-blodgett films of amphiphilic poly (propylene imine) dendrimers, J. Phys. Chem. C 111 (12) (2007) 4695–4701.
[36] T. Zhang, P.R. Dvornic, S.N. Kaganove, A comparative study of Amphiphilic PAMAM dendrimers at the air-water interface with different hydrophobe attachment groups, Langmuir 23 (21) (2007) 10589–10597.
[37] J.J. Giner-Casares, G. Brezesinski, H. Möhwald, Langmuir monolayers as unique physical models, Curr. Opin. Colloid Interface Sci. 19 (3) (2014) 176–182.
[38] E.G. Fernandes, N.C. Vieira, A.A. de Queiroz, F.E. Guimaraes, V. Zucolotto, Immobilization of poly (propylene imine) dendrimer/nickel phtalocyanine as nanostructured multilayer films to be used as gate membranes for SEGFET pH sensors, J. Phys. Chem. C 114 (14) (2010) 6478–6483.
[39] R.M. Iost, J.M. Madurro, A.G. Brito-Madurro, I.L. Nantes, L. Caseli, F.N. Crespilho, Strategies of nano-manipulation for application in electrochemical biosensors, Int. J. Electrochem. Sci. 6 (2011) 2965–2997.
[40] R.S. Navath, A.R. Menjoge, B. Wang, R. Romero, S. Kannan, R.M. Kannan, Amino acid-functionalized dendrimers with heterobifunctional chemoselective peripheral groups for drug delivery applications, Biomacromolecules 11 (6) (2010) 1544–1563.
[41] D.G. Mullen, M. Fang, A. Desai, J.R. Baker Jr., B.G. Orr, M.M. Banaszak Holl, A quantitative assessment of nanoparticle– ligand distributions: implications for targeted drug and imaging delivery in dendrimer conjugates, Acs Nano 4 (2) (2010) 657–670.

[42] H. Nagatani, T. Sakamoto, T. Torikai, T. Sagara, Encapsulation of anilinonaphthalenesulfonates in carboxylate-terminated PAMAM dendrimer at the polarized water| 1,2-dichloroethane interface, Langmuir 26 (22) (2010) 17686–17694.
[43] V. Biju, Chemical modifications and bioconjugate reactions of nanomaterials for sensing, imaging, drug delivery and therapy, Chem. Soc. Rev. 43 (3) (2014) 744–764.
[44] D.A. Tomalia, J.B. Christensen, U. Boas, Dendrimers, Dendrons, and Dendritic Polymers: Discovery, Applications, and the Future, Cambridge University Press, 2012.
[45] M. Marcos, R. Martín-Rapún, A. Omenat, J.L. Serrano, Highly congested liquid crystal structures: dendrimers, dendrons, dendronized and hyperbranched polymers, Chem. Soc. Rev. 36 (12) (2007) 1889–1901.
[46] M. Zhi-Mei, C. Si-Xue, Z. Xian-Zheng, W. Qing-Rong, R. Zhuo, Degradation and drug release property of star poly (ε-caprolactone) s with dendritic cores, J. Biomed. Mater. Res. B: Appl. Biomater. B 81 (2006) 40.
[47] S. Zhu, M. Hong, L. Zhang, G. Tang, Y. Jiang, Y. Pei, PEGylated PAMAM dendrimer-doxorubicin conjugates: in vitro evaluation and in vivo tumor accumulation, Pharm. Res. 27 (1) (2010) 161–174.
[48] S. Prakash, T. Chakrabarty, A.K. Singh, V.K. Shahi, Polymer thin films embedded with metal nanoparticles for electrochemical biosensors applications, Biosens. Bioelectron. 41 (2013) 43–53.
[49] Y. Xu, B. Zhang, Recent advances in porous Pt-based nanostructures: synthesis and electrochemical applications, Chem. Soc. Rev. 43 (8) (2014) 2439–2450.
[50] X. Hong, C. Tan, J. Chen, Z. Xu, H. Zhang, Synthesis, properties and applications of one-and two-dimensional gold nanostructures, Nano Res. 8 (1) (2015) 40–55.
[51] H. Duan, D. Wang, Y. Li, Green chemistry for nanoparticle synthesis, Chem. Soc. Rev. 44 (16) (2015) 5778–5792.
[52] S. Lin, L. Liu, J. Hu, Y. Liang, W. Cui, Nano Ag@ AgBr surface-sensitized Bi_2WO_6 photocatalyst: oil-in-water synthesis and enhanced photocatalytic degradation, Appl. Surf. Sci. 324 (2015) 20–29.
[53] S.-S. Kim, B.-H. Sohn, Template-assisted self-assembly of diblock copolymer micelles for non-hexagonal arrays of Au nanoparticles, RSC Adv. 6 (47) (2016) 41331–41339.
[54] V. Malgras, Q. Ji, Y. Kamachi, T. Mori, F.-K. Shieh, K.C. Wu, K. Ariga, Y. Yamauchi, Templated synthesis for nanoarchitectured porous materials, Bull. Chem. Soc. Japan (2015).
[55] A. Leiva, M. Méndez, M. Pino, D. Radić, In situ synthesis of gold nanoparticles at the air–water interface. Spontaneous reduction of Au (III) by poly (N-vinyl-2-pyrrolidone) monolayers, Eur. Polym. J. 49 (8) (2013) 2128–2137.
[56] X. Cao, C. Cheng, Y. Ma, C. Zhao, Preparation of silver nanoparticles with antimicrobial activities and the researches of their biocompatibilities, J. Mater. Sci.: Mater. Med. 21 (10) (2010) 2861–2868.
[57] P. Kumar Vemula, U. Aslam, V. Ajay Mallia, G. John, In situ synthesis of gold nanoparticles using molecular gels and liquid crystals from vitamin-C amphiphiles, Chem. Mater. 19 (2) (2007) 138–140.
[58] S. Nawaz, P. Carbone, Stability of amphiphilic dendrimers at the water/air interface, J. Phys. Chem. B 115 (42) (2011) 12019–12027.
[59] A.F. Stalder, T. Melchior, M. Müller, D. Sage, T. Blu, M. Unser, Low-bond axisymmetric drop shape analysis for surface tension and contact angle measurements of sessile drops, Colloids Surf. A: Physicochem. Eng. Aspects 364 (1) (2010) 72–81.
[60] J. Wang, W. Wang, P.A. Kollman, D.A. Case, Automatic atom type and bond type perception in molecular mechanical calculations, J. Mol. Graph. Model. 25 (2) (2006) 247–260.
[61] L. Martínez, R. Andrade, E.G. Birgin, J.M. Martínez, Packmol: a package for building initial configurations for molecular dynamics simulations, J. Comput. Chem. 30 (13) (2009) 2157–2164.
[62] K.J. Bowers, E. Chow, H. Xu, R.O. Dror, M.P. Eastwood, B.A. Gregersen, J.L. Klepeis, I. Kolossvary, M.A. Moraes, F.D. Sacerdoti, Scalable algorithms for molecular dynamics simulations on commodity clusters, in: SC 2006 Conference, Proceedings of the ACM/IEEE, IEEE, 2006, pp. 43-43.
[63] W. Humphrey, A. Dalke, K. Schulten, VMD: visual molecular dynamics, J. Mol. Graph. 14 (1) (1996) 33–38.
[64] H.J. Berendsen, J.v. Postma, W.F. van Gunsteren, A. DiNola, J. Haak, Molecular dynamics with coupling to an external bath, J. Chem. Phys. 81 (8) (1984) 3684–3690.
[65] S. Nosé, A unified formulation of the constant temperature molecular dynamics methods, J. Chem. Phys. 81 (1) (1984) 511–519.
[66] W.G. Hoover, Canonical dynamics: equilibrium phase-space distributions, Phys. Rev. A 31 (3) (1985) 1695.
[67] G.J. Martyna, D.J. Tobias, M.L. Klein, Constant pressure molecular dynamics algorithms, J. Chem. Phys. 101 (5) (1994) 4177–4189.
[68] M. Tuckerman, B.J. Berne, G.J. Martyna, Reversible multiple time scale molecular dynamics, J. Chem. Phys. 97 (3) (1992) 1990–2001.
[69] U. Essmann, L. Perera, M.L. Berkowitz, T. Darden, H. Lee, L.G. Pedersen, A smooth particle mesh Ewald method, J. Chem. Phys. 103 (19) (1995) 8577–8593.
[70] W.L. Jorgensen, D.S. Maxwell, J. Tirado-Rives, Development and testing of the OPLS all-atom force field on conformational energetics and properties of organic liquids, J. Am. Chem. Soc. 118 (45) (1996) 11225–11236.
[71] D.J. Price, C.L. Brooks III, A modified TIP3P water potential for simulation with Ewald summation, J. Chem. Phys. 121 (20) (2004) 10096–10103.
[72] A. Vergara-Jaque, J. Comer, L. Monsalve, F.D. González-Nilo, C. Sandoval, Computationally efficient methodology for atomic-level characterization of dendrimer–drug complexes: a comparison of amine-and acetyl-terminated PAMAM, J. Phys. Chem. B 117 (22) (2013) 6801–6813.
[73] P.K. Maiti, T. Cagin, S.-T. Lin, W.A. Goddard, Effect of solvent and pH on the structure of PAMAM dendrimers, Macromolecules 38 (3) (2005) 979–991.
[74] J. Xu, J. Reumers, J.R. Couceiro, F. De Smet, R. Gallardo, S. Rudyak, A. Cornelis, J. Rozenski, A. Zwolinska, J.-C. Marine, Gain of function of mutant p53 by coaggregation with multiple tumor suppressors, Nat. Chem. Biol. 7 (5) (2011) 285–295.
[75] T. Williams, C. Kelley, H. Broker, E. Merritt, J. Campbell, R. Cunningham, D. Denholm, G. Elber, R. Fearick, C. Grammes, Gnuplot 4.4: an interactive plotting program, Official gnuplot documentation, 2010. <http://sourceforge.net/projects/gnuplot>.
[76] A. Frisch, H. Hratchian, R. Dennington II, T. Keith, J. Millam, B. Nielsen, A. Holder, J. Hiscocks, GaussView Version 5.0. 8, Gaussian, Inc., Wallingford, CT, USA, 2009.
[77] S. Bonardd, M. Schmidt, M. Saavedra-Torres, A. Leiva, D. Radic, C. Saldías, Thermal and morphological behavior of chitosan/PEO blends containing gold nanoparticles, Exp. Theor. Stud. Carbohyd. Polym. 144 (2016) 315–329.
[78] H. Sekhar De, S. Krishnamurty, S. Pal, Understanding the reactivity properties of Au n ($6 \leqslant n \leqslant 13$) clusters using density functional theory based reactivity descriptors, J. Phys. Chem. C 114 (14) (2010) 6690–6703.
[79] M.P. Johansson, I. Warnke, A. Le, F. Furche, At what size do neutral gold clusters turn three-dimensional?, J Phys. Chem. C 118 (50) (2014) 29370–29377.
[80] X. Chen, S. Sun, F. Li, X. Wang, D. Xia, The interactions of oxygen with small gold clusters on nitrogen-doped graphene, Molecules 18 (3) (2013) 3279–3291.
[81] A.V. Marenich, S.V. Jerome, C.J. Cramer, D.G. Truhlar, Charge model 5: an extension of hirshfeld population analysis for the accurate description of molecular interactions in gaseous and condensed phases, J. Chem. Theory Comput. 8 (2) (2012) 527–541.
[82] A. Leiva, C. Saldías, C. Quezada, A. Toro-Labbé, F.J. Espinoza-Beltrán, M. Urzúa, L. Gargallo, D. Radic, Gold-copolymer nanoparticles: poly (ε-caprolactone)/poly (N-vinyl-2-pyrrolydone) Biodegradable triblock copolymer as stabilizer and reductant, Eur. Polym. J. 45 (11) (2009) 3035–3042.
[83] C. Saldías, Á. Leiva, S. Bonardd, C. Quezada, S. Saldías, M. Pino, A facile one-step synthesis of noble metal nanoparticles in DMSO using poly (ethylene glycol)-poly (ε-caprolactone) block copolymers, React. Funct. Polym. 96 (2015) 78–88.
[84] K.D.N. Vo, E. Guillon, L. Dupont, C. Kowandy, X. Coqueret, Influence of Au (III) interactions with chitosan on gold nanoparticle formation, J. Phys. Chem. C 118 (8) (2014) 4465–4474.
[85] X. Yin, X. Zhang, Q. Lin, Y. Feng, W. Yu, Q. Zhang, Metal-coordinating controlled oxidative degradation of chitosan and antioxidant activity of chitosan-metal complex, Arkivoc 9 (2004) 66–78.